Single-Molecule Detection of H_2O_2 Mediating Angiogenic Redox Signaling on Fluorescent Single-Walled Carbon Nanotube Array

Jong-Ho Kim,[†,‡] Chitta Ranjan Patra,[§,⊥] Jyoti R. Arkalgud,[†] Ardemis A. Boghossian,[†] Jingqing Zhang,[†] Jae-Hee Han,[†,¶] Nigel F. Reuel,[†] Jin-Ho Ahn,[†] Debabrata Mukhopadhyay,[§] and Michael S. Strano[†,*]

[†]Department of Chemical Engineering, Massachusetts Institute of Technology, Cambridge, Massachusetts 02139, United States, [‡]Department of Chemical Engineering, Hanyang University, Ansan 426-791, Republic of Korea, [§]Department of Biochemistry and Molecular Biology and Department of Biomedical Engineering, Mayo Clinic, Rochester, Minnesota 55905, United States, [⊥]Department of Chemical Biology, Indian Institute of Chemical Technology [IICT], Hyderabad, AP, 500607, India and [¶]Department of Energy IT, Kyungwon University, Seongnam, Gyeonggi-do 461-701, Republic of Korea

ABSTRACT Reactive oxygen species, specifically hydrogen peroxide (H_2O_2), activate signal transduction pathways during angiogenesis and therefore play an important role in physiological development as well as various pathophysiologies. Herein, we utilize a near-infrared fluorescent single-walled carbon nanotube (SWNT) sensor array to measure the single-molecule efflux of H_2O_2 from human umbilical vein endothelial cells (HUVEC) in response to angiogenic stimulation. Two angiogenic agents were investigated: the pro-angiogenic cytokine, vascular endothelial growth factor A (VEGF-A) and the recently identified inorganic pro-angiogenic factor, europium(III) hydroxide in nanorod form. The nanosensor array consists ofa SWNT embedded within a collagen matrix that exhibits high selectivity and sensitivity to single molecules of H_2O_2. A calibration from 12.5 to 400 nM quantifies the production of H_2O_2 at nanomolar concentration in HUVEC with 1 s temporal and 300 nm spatial resolutions. We find that the production of H_2O_2 following VEGF stimulation is elevated outside of HUVEC, but not for stimulation *via* nanorods, while increased generation is observed in the cytoplasm for both cases, suggesting two distinct signaling pathways.

KEYWORDS: single-walled carbon nanotube · near-infrared fluorescence · single-molecule detection · hydrogen peroxide · redox signaling · angiogenesis · europium(III) hydroxide nanorods

Angiogenesis is a process of new blood vessel creation from existing vasculature that plays an important role in physiological and pathophysiological processes such as wound healing, ischemic heart and limb disease, tumor growth and metastasis, rheumatoid arthritis, and atherosclerosis.[1−3] Vascular endothelial growth factor (VEGF) is a pro-angiogenic cytokine promoting proliferation, migration, and capillary formation of endothelial cells (EC).[4,5] It has been reported that VEGF signaling in EC induces the increased production of reactive oxygen species (ROS) intracellularly.[6,7] It is known that ROS serve an antimicrobial function[8] in addition to intracellular signaling.[9] Hydrogen peroxide (H_2O_2) is generated primarily from dismutation of superoxide produced by NADPH oxidase (Nox) in the EC membrane,[10] and mediates cellular signal transduction *via* oxidation of protein tyrosine phosphatases (PTP) and the activation of kinases and transcription factors during angiogenesis.[11−13] Among ROS, H_2O_2 is a dominant oxidant in cellular redox signaling processes due to its much longer lifetime (half-life, 1 ms) and higher concentration (steady-state level, 100 nM) than other ROS such as superoxide and hydroxyl radical.[9]

Recently, lanthanides have attracted interest as therapeutic tools to manipulate angiogenic signaling.[14] Specifically, europium(III) hydroxide nanorods show unique pro-angiogenic properties involving EC proliferation and vascular sprouting like other pro-angiogenic cytokines such as VEGF and basic fibroblast growth factor.[15] However, the mechanism of angiogenesis induction in EC for this inorganic nanomaterial remains unknown. In particular, a central question is whether H_2O_2 participates as an intercellular signaling molecule in addition to an intracellular signaling molecule during angiogenesis in EC. To this extent, a comparison of the redox signaling pathways between nanorods and VEGF may elucidate the angiogenic mechanism of the former. This mechanism may also inform the development of new therapeutic strategies for diseases in which angiogenesis plays an important role such as cardiovascular diseases and cancer.

Several approaches have been reported to detect cellular H_2O_2. Organic dye-based

* Address correspondence to strano@mit.edu.

Received for review May 24, 2011 and accepted September 7, 2011.

Published online September 07, 2011
10.1021/nn201904t

probes typically depend on chemical reaction to fluorescent products.[16−19] They often lack reversibility prohibiting observation of signaling over long times. Reversible probes for H_2O_2 detection remain an active area of research, with examples including genetically encoded fluorescent indicators[20] and europium-doped nanoparticles.[21] However, quantitative detection remains difficult[20] and selectivity toward H_2O_2 is often compromised.[21] These approaches also cannot quantify H_2O_2 efflux from cells, particularly at the single-molecule level necessary to resolve physiological signaling[9] in living cells. Therefore, there is still a longstanding need to develop probes capable of providing selective, spatiotemporal, and quantitative information of H_2O_2 production in living organisms in order to better understand its roles as a redox signaling molecule.

There are several promising applications of single-walled carbon nanotubes (SWNTs) to biological and medical research areas.[22−27] In particular, semiconducting SWNTs appear to be a suitable nanomaterial for fluorescent optical sensors[28−36] in biological and medical research due to their stable photoluminescence (PL)[37] in the near-infrared (nIR) region with no-photobleaching threshold,[38,39] which allows long exposures and integration times compared to other probes. SWNT PL is also sensitive to environmental changes including charge transfer[33,40,41] and local dielectric change,[29,42,43] which causes intensity alteration and photoemission shift. Recently, it has been demonstrated that nIR fluorescent SWNTs can detect small molecules even at the single-molecule level by monitoring the stepwise fluorescence quenching of single SWNT sensor.[44−47] In addition, we have shown that SWNTs embedded in collagen are able to selectively and reversibly detect H_2O_2 against other ROS.[45,46] However, it is a remaining challenge to quantitatively detect small molecules like H_2O_2 at nanomolar concentrations produced from living cells, particularly for the elucidation of diverse signaling pathways.

Herein, we apply our SWNT/collagen sensor to the problem of single-molecule detection of H_2O_2 efflux during angiogenic signaling triggered by VEGF or the artificial pro-angiogenic factor, europium(III) hydroxide nanorods, in EC. The SWNT/collagen sensor is calibrated for H_2O_2 at nanomolar concentration to quantify its production in living EC stimulated by VEGF or nanorods. The production of H_2O_2 outside EC is quantitatively and spatiotemporally measured for all stimulations inducing angiogenesis on the SWNT/collagen sensor, which enables us to understand the mechanism of its generation for angiogenic redox signaling in living EC. We find that H_2O_2 is mainly produced near the EC membrane after VEGF stimulation while it is generated in the EC cytoplasm for nanorods stimulation during angiogenesis, indicating distinct signaling pathways.

RESULTS AND DISCUSSION

To quantitatively detect H_2O_2 generated from human umbilical vein endothelial cells (HUVEC) for angiogenic signaling (Figure 1a), we first calibrated the SWNT/collagen sensor for H_2O_2 at nanomolar concentrations in PBS. This SWNT/collagen sensor is able to selectively detect H_2O_2 *via* electron transfer from the valence band of SWNT to LUMO of H_2O_2, which is proved by the diminution of the SWNT absorption and the oxidation potential (1.8 V) of hydrogen peroxide for the formation of a reduced product (H_2O) that is located below the potential of the valence band. The SWNT/collagen sensor array was prepared by slowly drying the diluted solution of collagen-suspended SWNTs (final concentration of SWNTs, 0.19 μg/mL) at room temperature on a glass-bottomed Petri dish as previously described.[45] As shown in Figure 1b, an area of 580 $\times$ 580 nm^2 (inset: 2 $\times$ 2 pixels in a diffraction-limited image) corresponds to a single SWNT, which is distinctly distributed on the glass surface of a Petri dish. The sensor array showed a very bright nIR fluorescence when it was observed by the nIR fluorescence microscope with a 100x TIRF objective (excitation with 658 nm laser). In addition, the nIR fluorescence of the SWNT/collagen sensor is very stable without fluctuation in the absence of H_2O_2 during measurement for 20 min as shown in the fluorescence time-trace (Figure 1c, without H_2O_2). However, stepwise fluorescence quenching is clearly observed upon addition of H_2O_2 (50 μM) into the solution (Figure 1c, H_2O_2 addition), indicating single-molecule adsorption of H_2O_2 on the sidewall of a single SWNT. These fluorescence time-traces demonstrate that the sensor responds predominately to H_2O_2. Next, we added serially diluted solutions of H_2O_2 at nanomolar concentrations from 12.5 to 400 nM into the SWNT/collagen sensor in PBS in order to obtain a calibration curve for the local H_2O_2 concentration. After the fluorescence image was monitored in real-time for 20 min upon the addition of H_2O_2, 100 diffraction-limited spots (2 $\times$ 2 pixels/spot, 100 SWNT sensors, Figure 1b) were selected in the order of the highest to lowest intensity for analysis as reported previously.[45] Then, we calculated the number of fluorescence transitions observed as a function of H_2O_2 concentration. To calculate the number of transitions corresponding to H_2O_2 adsorption on each selected SWNT, each time-trace was subjected to an error-minimizing step-finding algorithm[48] where the intrinsic steps in intensity are easily identified within the noise. Best-fit traces were obtained in a manner analogous to linear regression, where the final regression minimized the error between the fitted curve and the experimental data. On the basis of the best-fit traces, the number of transitions was calculated. As shown in the representative traces (Figure 2a−d, Supporting Information, Figure S1), there was stochastic variation in the number

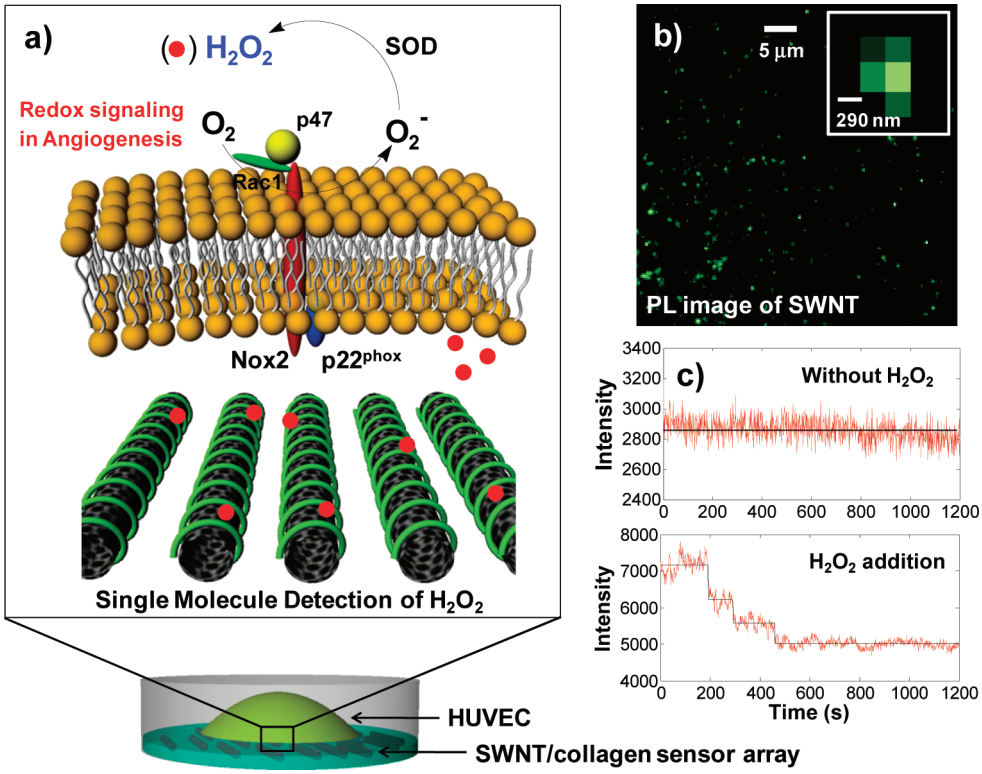

Figure 1. Single-molecule detection of H_2O_2 mediating aniogenic redox signaling. (a) Schematic diagram of H_2O_2 production in angiogenesis and sensing platform. (b) nIR fluorescence image of a SWNT/collagen sensor array showing emission from single isolated SWNT sensors. Inset: diffraction-limited spot (2 × 2 pixels) corresponding to a single SWNT. (c) Representative fluorescence time-traces (red) in PBS with and without H_2O_2 (50 μM), showing clear stepwise fluorescence quenching.

of states observed in 1200 s traces from 3 to 10 for single-molecule adsorption of H_2O_2; however, it is clear that the fluorescent responses show sensitivities down to the single-molecule level. We find that the total number of transitions observed per unit time is the optimal way to construct a calibration that relates to the concentration above the sensors. Figure 2e shows that the number of transitions increases with an increase in the concentration of H_2O_2 up to 100 nM (Figure 2e). We found that the automated procedure described above tended to overestimate the number of actual transitions, leading to a sharper calibration curve than what one obtains by visual inspection of the trace. Therefore, we sent the traces having clear and sharp transitions selected by visual inspection to the algorithm in order to count the number of transitions and to create the calibration curve. A more accurate calibration curve was constructed in this manner and demonstrates a more uniform, monotonic trend. As depicted in Figure 2f, the total number of transitions shows better correlation with the concentration of H_2O_2 in the range of 12.5−400 nM. Since the steady-state concentration of H_2O_2 for signaling in living cells is approximately 100 nM within the cell,[9] the calibration of the SWNT/collagen sensor at nanomolar concentration can be effectively applied to quantification of its production related to angiogenic signaling in HUVEC.

We then utilized this sensor to quantitatively detect H_2O_2 generated from angiogenic redox signaling in living HUVEC to investigate the mechanism of its production stimulated by either VEGF or europium(III) hydroxide [$Eu(OH)_3$] nanorods as pro-angiogenic factors. In EC, VEGF stimulates EC proliferation by producing H_2O_2,[11−13] as a critical step in angiogenesis. It is observed that nanorod stimulation at 10 μg/mL results in an increase in EC proliferation and viability compared to unstimulated control, confirmed by MTS assay[49] as shown in Figure 3a. This result clearly indicates that nanorods stimulation promotes HUVEC proliferation essential for angiogenesis as VEGF. One of the important signaling pathways for angiogenesis is the activation of mitogen-activated protein kinases (MAPK). Thus, we investigated the level of total MAPK and phosphomapkinase by Western blot analysis in HUVEC treated with europium(III) hydroxide nanorods in the presence or absence of manganese(III) tetrakis-(4-benzoic acid)porphyrin chloride (MnTBAP)[50,51] as a mimic of cell-permeable superoxide dismutase (SOD)[52,53] that is an enzyme to catalyze the dismutation of superoxide into H_2O_2 in living cells. VEGF stimulation was used as a positive control. As shown in Figure 3b, there is a significant increase in MAPK phosphorylation when HUVEC was treated with VEGF. Interestingly, $Eu(OH)_3$ nanorod stimulation of HUVEC in the presence of MnTBAP increases phosphorylation of

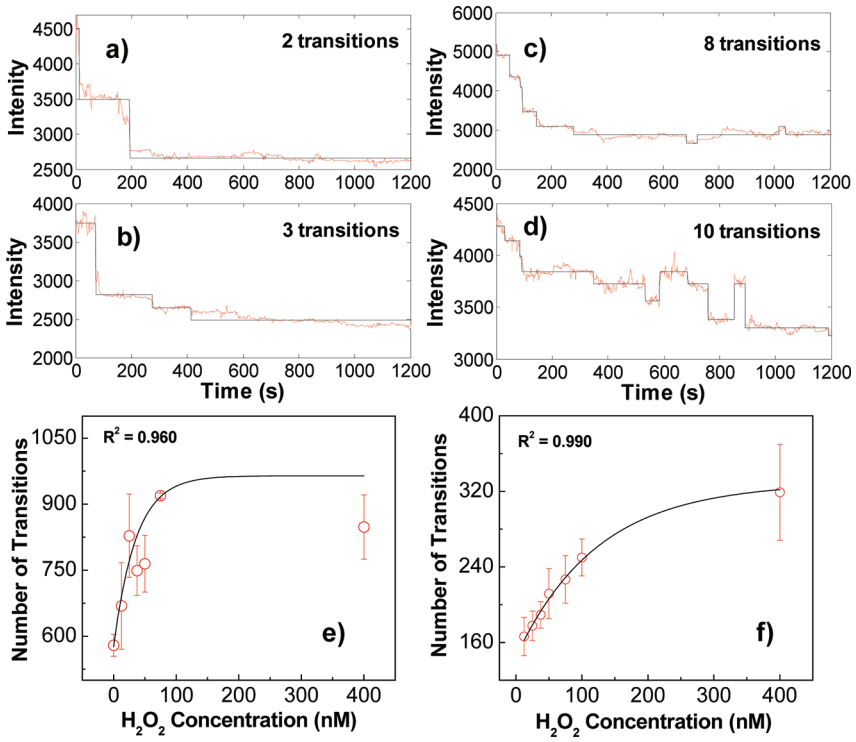

Figure 2. Calibration of SWNT/collagen sensor for H_2O_2. Representative fluorescence time-trace (red) monitored for 20 min showing (a) 2, (b) 3, (c) 8, and (d) 10 transitions upon addition of H_2O_2 (400 nM) in PBS. (e) Correlation of the total number of transitions with H_2O_2 concentration for all 100-SWNT sensors. (f) Calibration curve for H_2O_2 at nanomolar concentration from 12.5 to 400 nM after selecting the traces having sharp real-transitions, showing that the total number of transitions increases with increasing H_2O_2 concentration. A flat part and a sharp drop in a black line of each trace are considered as a state and a transition, respectively.

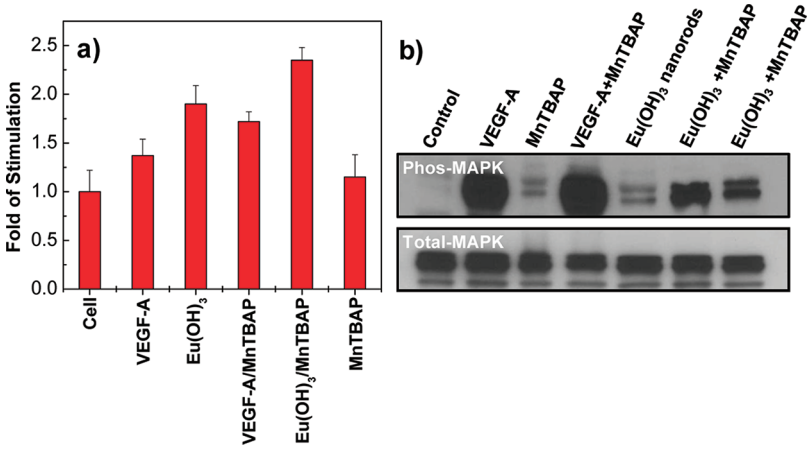

Figure 3. Effect of VEGF-A and $Eu(OH)_3$ nanorods stimulation on angiogenesis of HUVEC. (a) Cell proliferation and viability results for VEGF-A (10 ng/mL) and nanorods (10 μg/mL) stimulation, showing that the nanorods promote an increase in HUVEC proliferation similar to VEGF-A. MTS assay was conducted. (b) Western blot analysis for phosphomapkinase (phos-MAPK) and total mapkinase after VEGF-A and nanorods stimulation in HUVEC, showing the upregulation of phos-MAPK in the presence of nanorods/MnTBAP as well as VEGF-A for 15 and 30 min treatment, respectively. HUVEC was treated with VEGF-A for 5 min, and with nanorods for 15 and 30 min, respectively (last two lanes in a gel) in the presence or absence of MnTBAP.

MAPK similar to the case of VEGF stimulation and part of the known signaling pathway in angiogenesis.[54−57] These results clearly verify that these nanorods have pro-angiogenic properties in EC, similar to other cytokines such as VEGF.

To detect H_2O_2 generated from HUVEC stimulated by VEGF or $Eu(OH)_3$ nanorods, the cells were replated onto the SWNT/collagen sensor array in a Petri dish filled with a complete EBM medium. After cell adhesion on the sensor array, the complete EBM medium was replaced with a serum-starving one (0.2% fetal bovine serum). The cells on the sensor array in the serum-starving medium were incubated further for 12 h at 37 °C, and then stimulated with VEGF (10 ng/mL) or the

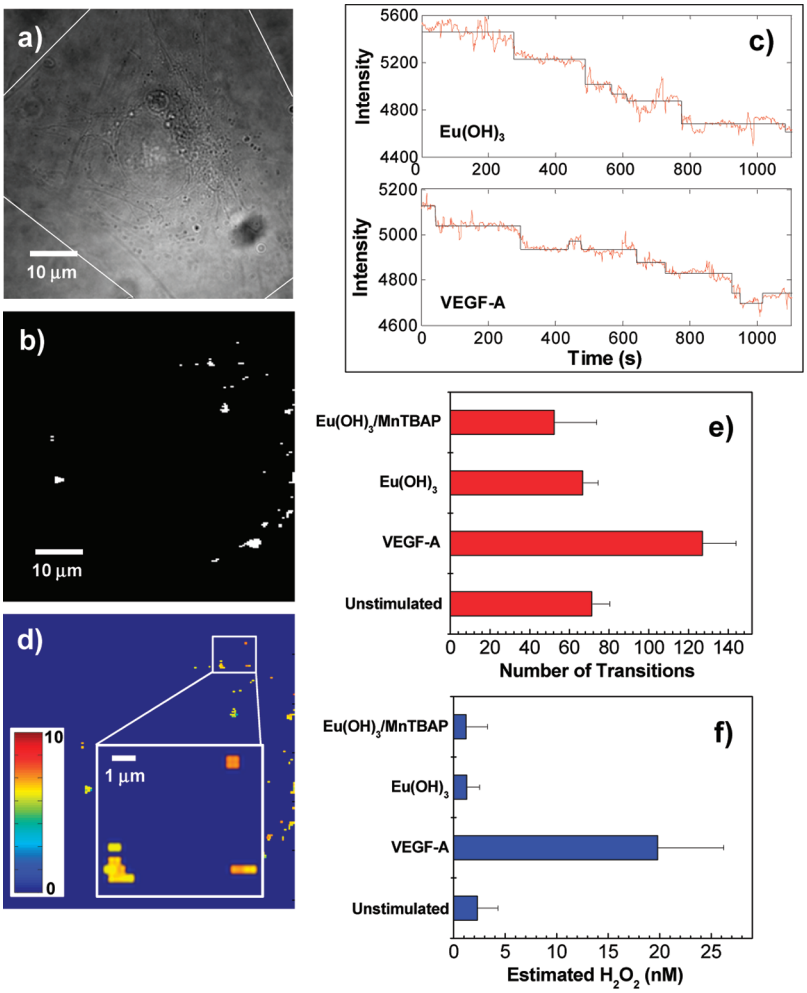

Figure 4. Single-molecule detection of H_2O_2 produced from living HUVEC for angiogenic redox signaling. (a) White-light picture of single cell stimulated by VEGF-A on the top of SWNT/collagen sensor array. The white lines indicate the outline of a single cell. (b) The 100 diffraction-limited spots of SWNTs underneath a cell, which are selected for analysis of fluorescence response to H_2O_2. (c) Representative fluorescence time-traces (red) selectively responding to H_2O_2 produced under VEGF-A and $Eu(OH)_3$ nanorods stimulation in HUVEC, showing stepwise quenching. (d) Spatial distribution plot of the number of transitions after VEGF-A stimulation on HUVEC. (e) The total number of transitions calculated from 100-selected SWNTs over the course of 20 min upon treatment of stimuli such as VEGF-A, $Eu(OH)_3$ nanorods, and $Eu(OH)_3$/MnTBAP to HUVEC. (f) Estimated concentration of H_2O_2 produced from HUVEC stimulated by VEGF-A, $Eu(OH)_3$ nanorods and $Eu(OH)_3$/MnTBAP using the calibration curve (Figure 2f).

nanorods (10 μg/mL). The nIR fluorescence response of the sensors underneath a single cell was then monitored in real-time for 20 min to quantitatively detect H_2O_2 produced from HUVEC and analyzed by the algorithm to calculate flux. Figure 4a shows the white-light image of a single HUVEC stimulated with VEGF on the top of the SWNT/collagen array, showing normal morphology. As shown in Supporting Information, Figure S2, the morphology of the cells stimulated with the $Eu(OH)_3$ nanorods is also normal and similar to the VEGF-stimulated case. Hence, we observe no apparent cytotoxicity from nanorod exposure, as assessed in MTS assay (Figure 3a). Figure 4b shows the image of 100 brightest SWNT sensors underneath a single cell to locate individual SWNTs (2 $\times$ 2 pixels). As shown in the intensity time-traces (Figure 4c, red), the stepwise fluorescence quenching of SWNT/collagen sensors occurs underneath a cell stimulated by VEGF or $Eu(OH)_3$ nanorods, demonstrating that the sensor recognizes H_2O_2 outside of HUVEC after stimulations. On the basis of this stepwise quenching, we can calculate the number of transitions on each single sensor and generate the spatial map of H_2O_2 flux around the HUVEC (Figure 4d). Sensors at different locations are observed to have different numbers of transitions. This array of nanosensors is unique in that it is capable of providing spatial information of H_2O_2 production at the single cell level.

Next, we quantitatively compared the total number of transitions for a stimulated cell to one for an unstimulated cell. As shown in Figure 4e, the number of transitions (71 $\pm$ 9) for the unstimulated cell constitutes a background signal. This background was observed for the case of A431 cells in a recent study

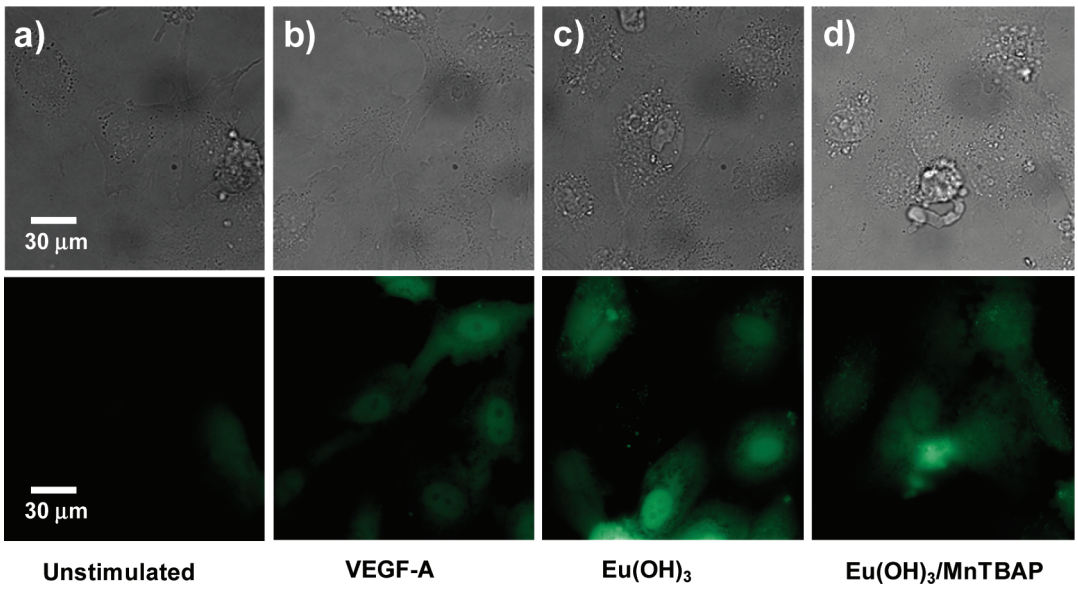

Figure 5. Intracellular detection of H_2O_2 in HUVEC after stimulation: white-light picture of cells and fluorescence image for (a) unstimulated one, (b) for VEGF-A, (c) for $Eu(OH)_3$ nanorods, (d) for $Eu(OH)_3$/MnTBAP. The results show that H_2O_2 production increases in the cytoplasm after stimulation. Carboxy-H_2DCFDA (25 μM) was used for detection of H_2O_2 inside of cells.

of EGFR signaling.[46] Unstimulated cells can produce H_2O_2 as redox signaling molecules for other physiological responses, and also as a part of cell respiration. In this case, Nox has been implicated in the basal production of H_2O_2 in the HUVEC membrane as suggested before,[46,58,59] as a major source of ROS during angiogenesis.[6,11,12] For VEGF stimulation, the total number of transitions (127 $\pm$ 17) observed for the same period of time (20 min, 100 SWNTs) is statistically greater than that of the unstimulated case (Figure 4e). We conclude that VEGF induces the elevated efflux of H_2O_2 near the cell membrane for angiogenic signaling to promote the cell proliferation and the phosphorylation of MAPK in HUVEC as shown in Figure 3. The increased production of H_2O_2 after VEGF stimulation in HUVEC is attributed to the Nox-dependent signaling pathway activated by the growth factor, VEGF, mainly taking place in the cell membrane as demonstrated before.[6,12,60] In contrast, the SWNT/collagen array underneath HUVEC stimulated by $Eu(OH)_3$ nanorods shows no increase in the total number of transitions (67 $\pm$ 8) compared to unstimulated control. Additionally, we added MnTBAP (20 μg/mL)[50,51] to the $Eu(OH)_3$ nanorods-stimulated cell as a mimic of SOD.[52,53] As shown in Figure 4e, no increase in the total number of transitions (53 $\pm$ 21) over control is observed, even after additional MnTBAP stimulation. We conclude that H_2O_2 production in the HUVEC near the cell membrane does not appear to occur in the case of nanorods stimulation. Next, we quantitatively estimated the concentration of H_2O_2 production induced by VEGF or nanorods stimulation using the calibration curve (Figure 2f) based on the total number of transitions. As shown in Figure 4f, it was found that 20 nM of H_2O_2 is generated outside of the cells after VEGF stimulation, which is 10 times higher than the background concentration (2 nM) without stimulation. However, for the nanorods stimulation, 1.5 nM of H_2O_2 appears to be generated outside of the cell membrane, which is similar to the unstimulated case. Therefore, we can expect that the production mechanism of H_2O_2 triggered by $Eu(OH)_3$ nanorods for angiogenic redox signaling might be different from one stimulated by VEGF in HUVEC.

To investigate intracellular production of H_2O_2 following nanorod stimulation, we utilized the organic fluorescent probe, carboxy-H_2DCFDA,[61] to detect H_2O_2 in the cytoplasm of HUVEC. After the cells were stimulated with VEGF, nanorods, or nanorods/MnTBAP, carboxy-H_2DCFDA (25 μM) was incubated for 30 min at 37 °C. As shown in Figure 5, the VEGF stimulation leads to fluorescence increase in the cytoplasm of HUVEC compared to unstimulated control, indicating that H_2O_2 is increased by VEGF-induced signaling inside HUVEC as well as outside near the cell membrane, as detected by the SWNT/collagen sensor. Additionally, the fluorescence increase is also observed in the cytoplasm after $Eu(OH)_3$ nanorods or nanorods/MnTBAP stimulation compared to one in the absence of stimulation. We conclude that the production of H_2O_2 is elevated inside HUVEC upon nanorods stimulation although it is not observed outside near the cell membrane.

A notable difference between VEGF and nanorods stimulation is the location of H_2O_2 production in HUVEC according to the experimental results. The VEGF stimulation leads to Nox activation in the cell membrane to produce superoxide that is quickly converted into H_2O_2 by extracellular SOD.[58,59,62] This proximity production of H_2O_2 near VEGFR in the cell

membrane is effectively detected by the SWNT/collagen sensor underneath the cells, which then promotes VEGF-induced angiogenic signaling *via* oxidation of PTP colocalized in caveolae/lipid rafts.[58] However, we can suggest that the mechanism of H_2O_2 production induced by $Eu(OH)_3$ nanorods in HUVEC is likely distinct from the case of VEGF. When we investigated the fate of the nanorods inside of the cells after stimulation, they appear to be amorphous (Supporting Information, Figure S3b).[15] The trivalent nanorods (Eu^{3+}) can be easily reduced to divalent Eu^{2+} in the cytoplasm as reported before,[21] which can result in the change in the nanorod crystal structure from hexagonal (Figure S3a) to amorphous phase after incubation inside cells for the certain period of time. Therefore, we can speculate that the nanorods could play a role as an oxidant to directly inactivate PTP or phosphatase and tensin homologue (PTEN) in the cytoplasm *via* oxidation of cysteine, which leads to the increase of mitochondrial H_2O_2 production.[63] The diffusion of H_2O_2 generated in the cytoplasm across the HUVEC membrane is so limited that it could not be effectively detected by SWNT/collagen sensor outside cells.[64] This proposed mechanism for H_2O_2 production stimulated by $Eu(OH)_3$ nanorods can be supported by its increased production in the cytoplasm, but not outside near the cell membrane. Further efforts will explore these distinct signaling mechanisms in more detail.

In summary, we show that a fluorescent SWNT/collagen sensor selective to H_2O_2 is able to quantitatively detect H_2O_2 signaling from live HUVEC after stimulation by the growth factor, VEGF and the artificial pro-angiogenic factor, $Eu(OH)_3$ nanorods. Indeed, the detection of the spatial and temporal production of H_2O_2 from HUVEC enables the signaling mechanisms associated with each growth factor to be examined in greater detail. The quantitative detection of H_2O_2 is used to assess the mechanism of its production for two different stimulations, suggesting that it is induced near the membrane for the VEGF stimulation, but in the cytoplasm for the nanorods case. This is the first demonstration to quantitatively detect H_2O_2 at nanomolar concentration generated from the living organisms to decipher complex redox signaling pathways in relation to angiogenesis.

METHODS

Preparation of SWNT/Collagen Sensor Array. A 1 mg portion of SWNT was added in 1 mL of collagen solution (3.41 mg/mL) containing 0.02 M of acetic acid, and the resulting mixture was sonicated for 10 min in an ice bath using a probe-tip sonicator (40% amplitude, 10 W). The suspension was then centrifuged for 3 h at 16 300 *g*, and the supernatant was decanted. A 20 μL portion of collagen-suspended SWNT solution was added to 40 μL of collagen solution (3.41 mg/mL), and the resulting solution was diluted with an acetic acid solution (0.02 M, 4.14 mL). A 400 μL portion of final SWNT solution (0.19 μg/mL SWNT) was added in each Petri dish and gently dried at room temperature for 20 h. Before being used for cellular experiments, it was extensively washed with water and PBS (pH 8).

Calibration of SWNT/Collagen Sensor for H_2O_2 and Data Analysis. Before experiments, the sensor was washed several times with phosphate buffer solution (PBS) (pH 7.4). A 2 mL portion of PBS was added to the sensor in a Petri dish, which was placed on the top of the nIR fluorescence microscope (Carl Zeiss, Axiovert 200) attached with a 2D InGaAs array (Princeton Instruments OMA 2D) with a 100× TIRF objective (658 nm laser excitation). After focusing on the sensor, the fluorescence response was imaged and monitored over time at 1 s/frame over the course of 1200 s upon addition of 88 μL of a 9.11 μM-H_2O_2 solution (final concentration, 400 nM). A solution of H_2O_2 was serially diluted from 400 to 12.5 nM in order to obtain the calibration curve. The calculation for the number of transitions from a movie monitoring the entire SWNT film fluorescence over time was determined using an algorithm. In the first step, a MATLAB routine selected 100 diffraction-limited spots (2 × 2 pixels) in the nIR images, in the order of the highest intensity to the lowest intensity. Each obtained time-trace was then subjected to an error-minimizing step-finding algorithm where the intrinsic steps in intensity can be identified within noisy data. To detail this further, the best-fit traces were obtained in a manner analogous to linear regression, where idealized traces exhibiting minimized error deviation from the experimental traces were selected. Specifically, the experimental trace was initially fit to a flat trace with a value equal to the mean intensity value of the experimental trace. Next, the algorithm assumes the existence of a single step where the value prior to the step is the mean intensity of the trace before the transition, and the value after the step is the mean intensity of the trace after the transition. The location of this step is iteratively fit at each time location within the trace, and the trace resulting in the best fit is selected. Once the location of the first transition is determined, the locations of the second and third steps are determined similarly by analyzing the bisections separately. In the region prior to this first transition, the algorithm once more assumes the existence of a step and determines its location by iteratively fitting the step to each time location prior to the transition. A similar analysis was performed to the second bisection or the region after the first transition, where the algorithm once more assumes the existence of a step and determines its location. The algorithm continues fitting steps to the bisections until the best fit is obtained. Finally, the number of transitions was calculated. To obtain the calibration curve for H_2O_2 (Figure 2f), the traces having sharp real-transitions were selected by going through all traces of 100 SWNT sensors with eyes, and then the selected trances were sent to the algorithm to calculate the total number of transitions. The fitting equation for the calibration curve is shown below (Eq. 1).

$$y = -235.57 \exp\left(\frac{-x}{63.548}\right) + 300 \quad (1)$$

Western Blot Analysis for Phosphomapkinase (phos-MAPK) and Total Mapkinase. HUVEC was cultured at 100 mm Petri dishes for 24 h at 37 °C and 5% CO_2 in EBM complete media with 5% FBS. The next day, cells were grown to 70% confluence, and then incubated with EBM starved media for another 24 h at 37 °C. They were then treated with $Eu(OH)_3$ nanorods (10 μg/mL), VEGF (10 ng/mL), and MnTBAP (20 μg/mL). After treatment, the harvested HUVEC was washed with cold PBS three times and lysed with ice-cold radioimmunoprecipitation (RIPA) buffer with freshly added 0.01% protease inhibitor cocktail (Sigma). After cells were incubated on ice for 10 min, the cell lysis was centrifuged at 14 000 rpm for 15 min at 4 °C. After protein estimation using the photometric method, 20 μg of protein was loaded on a 10% (Tris-HCl) polyacrylamide gel and transferred to nitrocellulose membrane. After the membrane was blocked

in 5% BSA in Tris buffered saline (TBS) containing Tween-20 for 1 h, it was incubated for 2 h with monoclonal mouse P-p44/42 (mouse mAb) and mapkinase (rabbit p44/42 MAPK) for phospho-MAP kinase upregulation and total MAP kinase. Finally, the membrane was incubated with HRP-coupled secondary antibodies (antimouse IgG or antirabbit IgG-HRP) at 25 °C for 45 min. The proteins were visualized using a chemiluminescent substrate.

Single-Molecule Detection of H_2O_2 Generated from Living HUVEC. After primary HUVEC confluent was over 90%, a compete EBM medium was removed from a flask. After washing cells with PBS twice, a 1.5 mL portion of trypsin/EDTA solution was added into the flask and incubated for 5 min at 37 °C. After the addition of 1.5 mL of trypsin neutralizing solution to the cells, they were centrifuged down in a microcentrifuge tube for 5 min at 1500 rpm. The supernatant was removed from the tube, and 1 mL of complete EBM medium was added. After gently mixing the cells, 50 μL of the cell solution was added into the SWNT/collagen sensor array in a Petri dish filled with 2 mL of a complete EBM medium. The cells were incubated to adhere on the top of the sensor array for 12 h at 37 °C. The complete EBM medium was then replaced to a serum-starving EBM medium (0.2% FBS), and incubated further for 12 h. Finally, the cells were treated with each stimulus such as VEGF-A (10 ng/mL), $Eu(OH)_3$ nanorods (10 μg/mL), and $Eu(OH)_3$/MnTBAP (20 μg/mL) in L-15 medium not containing FBS. The fluorescence response to H_2O_2 generated from the cells was imaged, monitored, and analyzed as described above for calibration of the sensor.

Acknowledgment. This work was supported by a Beckman Young Investigator Award to MSS and the National Science Foundation. A seed grant from the Center for Environmental Health and Science at MIT is also appreciated. J. H. Kim is grateful for the postdoctoral fellowship from the Korea Research Foundation Grant funded by the Korean Government (MOEHRD) (KRF-2007-357-D00086). C.R.P. is grateful to DST, Government of India, New Delhi, for the award of "Ramanujan Fellowship" grant (GAP 0305\DST\CP). This work was also supported by National Institutes of Health (NIH) grants HL70567 and CA150190 and a generous gift from Bruce and Martha Atwater to D.M.

Supporting Information Available: Materials, experimental procedures for MTS assay, and intracellular detection of H_2O_2 in HUVEC, Figure S1 for representative traces for each concentration of H_2O_2 from 12.5 to 400 nM, Figure S2 for single-molecule detection of H_2O_2 and Figure S3 for TEM images of $Eu(OH)_3$ nanorods. This material is available free of charge *via* the Internet at http://pubs.acs.org.

REFERENCES AND NOTES

1. Folkman, J. Angiogenesis in Cancer, Vascular, Rheumatoid and Other Disease. *Nat. Med.* **1955**, *1*, 27–31.
2. Risau, W. Mechanisms of Angiogenesis. *Nature* **1997**, *386*, 671–674.
3. Basu, S; Nagy, J. A.; Pal, S.; Vasile, E.; Eckelhoefer, I. A.; Bliss, V. S.; Manseau, E. J.; Dasgupta, P. S.; Dvorak, H. F.; Mukhopadhyay, D. The Neurotransmitter Dopamine Inhibits Angiogenesis Induced by Vascular Permeability Factor/Vascular Endothelial Growth Factor. *Nat. Med.* **2011**, *7*, 569–574.
4. Cross, M. J.; Dixelius, J.; Matsumoto, T.; Claesson-Welsh, L. VEGF-Receptor Signal Transduction. *Trends Biochem. Sci.* **2003**, *28*, 488–494.
5. Coultas, L.; Chawengsaksophak, K.; Rossant, J. Endothelial Cells and VEGF in Vascular Development. *Nature* **2005**, *438*, 937–945.
6. Ushio-Fukai, M. Redox Signaling in Angiogenesis: Role of NADPH Oxidase. *Cardiovasc. Res.* **2006**, *71*, 226–235.
7. Miller, T. W.; Isenberg, J. S.; Roberts, D. D. Molecular Regulation of Tumor Angiogenesis and Perfusion *via* Redox Signaling. *Chem. Rev.* **2009**, *109*, 3099–3124.
8. Finkel, T. Oxidant Signals and Oxidative Stress. *Curr. Opin. Cell Biol.* **2003**, *15*, 247–254.
9. D'Autreaux, B.; Toledano, M. B. ROS as Signalling Molecules: Mechanisms that Generate Specificity in ROS Homeostasis. *Nat. Rev. Mol. Cell Biol.* **2007**, *8*, 813–824.
10. Juarez, J. C.; Manuia, M.; Burnett, M. E.; Betancourt, O.; Boivin, B.; Shaw, D. E.; Tonks, N. K.; Mazar, A. P.; Donate, F. Superoxide Dismutase 1 (SOD1) is Essential for H_2O_2-mediated Oxidation and Inactivation of Phosphatases in Growth Factor Signaling. *Proc. Natl. Acad. Sci. U.S.A.* **2008**, *105*, 7147–7152.
11. Rhee, S. G. H_2O_2, A Necessary Evil for Cell Signaling. *Science* **2006**, *312*, 1882–1883.
12. Ushio-Fukai, M.; Nakamura, Y. Reactive Oxygen Species and Angiogenesis: NADPH Oxidase as Target for Cancer Therapy. *Cancer Lett.* **2008**, *266*, 37–52.
13. Frey, R. S.; Ushio-Fukai, M.; Malik, A. B. NADPH Oxidase-Dependent Signaling in Endothelial Cells: Role in Physiology and Pathophysiology. *Antioxid. Redox Signal.* **2009**, *11*, 791–810.
14. Fricker, S. P. The Therapeutic Application of Lanthanides. *Chem. Soc. Rev.* **2006**, *35*, 524–533.
15. Patra, C. R.; Bhattacharya, R.; Patra, S.; Vlahakis, N. E.; Gabashvili, A.; Koltypin, Y.; Gedanken, A.; Mukherjee, P.; Mukhopadhyay, D. Pro-angiogenic Properties of Europium(III) Hydroxide Nanorods. *Adv. Mater.* **2008**, *20*, 753–765.
16. Miller, E. W.; Albers, A. E.; Pralle, A.; Isacoff, E. Y.; Chang, C. J. Boronate-Based Fluorescent Probes for Imaging Cellular Hydrogen Peroxide. *J. Am. Chem. Soc.* **2005**, *127*, 16652–16659.
17. Hempel, S. L.; Buettner, G. R.; O'Malley, Y. Q.; Wessels, D. A.; Flaherty, D. M. Dihydrofluorescein Diacetate Is Superior for Detecting Intracellular Oxidants: Comparison with 2′,7′-Dichlorodihydrofluorescein Diacetate, 5(and 6)-Carboxy-2′,7′-Dichlorodihydrofluorescein Diacetate, and Dihydrorhodamine 123. *Free Radic. Biol. Med.* **1999**, *27*, 146–159.
18. Miller, E. W.; Tulyathan, O.; Isacoff, E. Y.; Chang, C. J. Molecular Imaging of Hydrogen Peroxide Produced for Cell Signaling. *Nat. Chem. Biol.* **2007**, *3*, 349–349.
19. Lee, D.; Khaja, S.; Velasquez-Castano, J. C.; Dasari, M.; Sun, C.; Petros, J.; Taylor, W. R.; Murthy, N. *In Vivo* Imaging of Hydrogen Peroxide with Chemiluminescent Nanoparticles. *Nat. Mater.* **2007**, *6*, 765–769.
20. Belousov, V. V.; Fradkov, A. F.; Lukyanov, K. A; Staroverov, D. B.; Shakhbazov, K. S.; Terskikh, A. V.; Lukyanov, S. Genetically Encoded Fluorescent Indicator for Intracellular Hydrogen Peroxide. *Nat. Methods* **2006**, *3*, 281–286.
21. Casanova, D.; Bouzigues, C.; Nguyen, T. L.; Ramodiharilafy, R. O.; Bouzhir-Sima, L.; Gacoin, T.; Boilot, J. P.; Tharaux, P. L.; Alexandrou, A. Single Europium-Doped Nanoparticles Measure Temporal Pattern of Reactive Oxygen Species Production Inside Cells. *Nat. Nanotechnol.* **2009**, *4*, 581–585.
22. Cherukuri, P.; Bachilo, S. M.; Litovsky, S. H.; Weisman, R. B. Near-Infrared Fluorescence Microscopy of Single-Walled Carbon Nanotubes in Phagocytic Cells. *J. Am. Chem. Soc.* **2004**, *126*, 15638–15639.
23. Cherukuri, P.; Gannon, C. J.; Leeuw, T. K.; Schmidt, H. K.; Smalley, R. E.; Curley, S. A.; Weisman, R. B. Mammalian Pharmacokinetics of Carbon Nanotubes Using Intrinsic Near-Infrared Fluorescence. *Proc. Natl. Acad. Sci. U.S.A.* **2006**, *103*, 18882–18886.
24. Liu, Z.; Cai, W. B.; He, L. N.; Nakayama, N.; Chen, K.; Sun, X. M.; Chen, X. Y.; Dai, H. J. *In Vivo* Biodistribution and Highly Efficient Tumour Targeting of Carbon Nanotubes in Mice. *Nat. Nanotechnol.* **2007**, *2*, 47–52.
25. Feazell, R. P.; Nakayama-Ratchford, N.; Dai, H.; Lippard, S. J. Soluble Single-Walled Carbon Nanotubes as Longboat Delivery Systems for Platinum(IV) Anticancer Drug Design. *J. Am. Chem. Soc.* **2007**, *129*, 8438–8439.
26. Jan, E.; Kotov, N. A. Successful Differentiation of Mouse Neural Stem Cells on Layer-by-Layer Assembled Single-Walled Carbon Nanotube Composite. *Nano Lett.* **2007**, *7*, 1123–1128.

27. Wang, L. B.; Chen, W.; Xu, D. H.; Shim, B. S.; Zhu, Y. Y.; Sun, F. X.; Liu, L. Q.; Peng, C. F.; Jin, Z. Y.; Xu, C. L.; *et al.* Simple, Rapid, Sensitive, and Versatile SWNT-Paper Sensor for Environmental Toxin Detection Competitive with ELISA. *Nano Lett.* **2009**, *9*, 4147–4152.
28. Barone, P. W.; Baik, S.; Heller, D. A.; Strano, M. S. Near-Infrared Optical Sensors Based on Single-Walled Carbon Nanotubes. *Nat. Mater.* **2005**, *4*, 86–92.
29. Heller, D. A.; Jeng, E. S.; Yeung, T. K.; Martinez, B. M.; Moll, A. E.; Gastala, J. B.; Strano, M. S. Optical Detection of DNA Conformational Polymorphism on Single-Walled Carbon Nanotubes. *Science* **2006**, *311*, 508–511.
30. Jeng, E. S.; Moll, A. E.; Roy, A. C.; Gastala, J. B.; Strano, M. S. Detection of DNA Hybridization Using the Near-Infrared Band-Gap Fluorescence of Single-Walled Carbon Nanotubes. *Nano Lett.* **2006**, *6*, 371–375.
31. Satishkumar, B. C.; Brown, L. O.; Gao, Y.; Wang, C. C.; Wang, H. L.; Doorn, S. K. Reversible Fluorescence Quenching in Carbon Nanotubes for Biomolecular Sensing. *Nat. Nanotechnol.* **2007**, *2*, 560–564.
32. Heller, D. A.; Jin, H.; Martinez, B. M.; Patel, D.; Miller, B. M.; Yeung, T. K.; Jena, P. V.; Hobartner, C.; Ha, T.; Silverman, S. K.; *et al.* Multimodal Optical Sensing and Analyte Specificity Using Single-Walled Carbon Nanotubes. *Nat. Nanotechnol.* **2009**, *4*, 114–120.
33. Kim, J. H.; Heller, D. A.; Jin, H.; Barone, P. W.; Song, C.; Zhang, J.; Trudel, L. J.; Wogan, G. N.; Tannenbaum, S. R.; Strano, M. S. The Rational Design of Nitric Oxide Selectivity in Single-Walled Carbon Nanotube Near-Infrared Fluorescence Sensors for Biological Detection. *Nat. Chem.* **2009**, *1*, 473–481.
34. Kim, J. H.; Ahn, J. H.; Barone, P. W.; Jin, H.; Zhang, J. Q.; Heller, D. A.; Strano, M. S. A Luciferase/Single-Walled Carbon Nanotube Conjugate for Near-Infrared Fluorescent Detection of Cellular ATP. *Angew. Chem., Int. Ed.* **2010**, *49*, 1456–1459.
35. Brege, J. J.; Gallaway, C.; Barron, A. R. Fluorescence Quenching of Single-Walled Carbon Nanotubes in SDBS Surfactant Suspension by Metal Ions: Quenching Efficiency as a Function of Metal and Nanotube Identity. *J. Phys. Chem. C* **2007**, *111*, 17812–17820.
36. Brege, J. J.; Gallaway, C.; Barron, A. R. Fluorescence Quenching of Single-Walled Carbon Nanotubes with Transition-Metal Ions. *J. Phys. Chem. C* **2009**, *113*, 4270–4276.
37. O'Connell, M. J.; Bachilo, S. M.; Huffman, C. B.; Moore, V. C.; Strano, M. S.; Haroz, E. H.; Rialon, K. L.; Boul, P. J.; Noon, W. H.; Kittrell, C.; *et al.* Band Gap Fluorescence from Individual Single-Walled Carbon Nanotubes. *Science* **2002**, *297*, 593–596.
38. Heller, D. A.; Baik, S.; Eurell, T. E.; Strano, M. S. Single-Walled Carbon Nanotube Spectroscopy in Live Cells: Towards Long-Term Labels and Optical Sensors. *Adv. Mater.* **2005**, *17*, 2793–2799.
39. Li, Q. W.; Zhang, X. F.; DePaula, R. F.; Zheng, L. X.; Zhao, Y. H.; Stan, L.; Holesinger, T. G.; Arendt, P. N.; Peterson, D. E.; Zhu, Y. T. Sustained Growth of Ultralong Carbon Nanotube Arrays for Fiber Spinning. *Adv. Mater.* **2006**, *18*, 3160–3163.
40. Strano, M. S.; Huffman, C. B.; Moore, V. C.; O'Connell, M. J.; Haroz, E. H.; Hubbard, J.; Miller, M.; Rialon, K.; Kittrell, C.; Ramesh, S.; Hauge, R. H.; *et al.* Reversible, Band-Gap-Selective Protonation of Single-Walled Carbon Nanotubes in Solution. *J. Phys. Chem. B* **2003**, *107*, 6979–6985.
41. O'Connell, M. J.; Eibergen, E. E.; Doorn, S. K. Chiral Selectivity in the Charge-Transfer Bleaching of Single-Walled Carbon Nanotube Spectra. *Nat. Mater.* **2005**, *4*, 412–418.
42. Walsh, A. G.; Vamivakas, A. N.; Yin, Y.; Cronin, S. B.; Unlu, M. S.; Goldberg, B. B.; Swan, A. K. Screening of Excitons in Single, Suspended Carbon Nanotubes. *Nano Lett.* **2007**, *7*, 1485–1488.
43. Choi, J. H.; Strano, M. S. Solvatochromism in Single-Walled Carbon Nanotubes. *Appl. Phys. Lett.* **2007**, *90*, 223114.
44. Cognet, L.; Tsyboulski, D. A.; Rocha, J. D. R.; Doyle, C. D.; Tour, J. M.; Weisman, R. B. Stepwise Quenching of Exciton Fluorescence in Carbon Nanotubes by Single-Molecule Reactions. *Science* **2007**, *316*, 1465–1468.
45. Jin, H.; Heller, D. A.; Kim, J. H.; Strano, M. S. Stochastic Analysis of Stepwise Fluorescence Quenching Reactions on Single-Walled Carbon Nanotubes: Single Molecule Sensors. *Nano Lett.* **2008**, *8*, 4299–4304.
46. Jin, H.; Heller, D. A.; Kalbacova, M.; Kim, J. H.; Zhang, J. Q.; Boghossian, A. A.; Maheshri, N.; Strano, M. S. Detection of Single-Molecule H_2O_2 Signalling from Epidermal Growth Factor Receptor Using Fluorescent Single-Walled Carbon Nanotubes. *Nat. Nanotechnol.* **2010**, *5*, 302–309.
47. Siitonen, A. J.; Tsyboulski, D. A.; Bachilo, S. M.; Weisman, R. B. Surfactant-Dependent Exciton Mobility in Single-Walled Carbon Nanotubes Studied by Single-Molecule Reactions. *Nano Lett.* **2010**, *10*, 1595–1599.
48. Kerssemakers, J. W. J.; Munteanu, E. L.; Laan, L.; Noetzel, T. L.; Janson, M. E.; Dogterom, M. Assembly Dynamics of Microtubules at Molecular Resolution. *Nature* **2006**, *442*, 709–712.
49. Mosmann, T. Rapid Colorimetric Assay for Cellular Growth and Survival-Application to Proliferation and Cyto-toxicity Assays. *J. Immunol. Methods* **1983**, *65*, 55–63.
50. Faulkner, K. M.; Liochev, S. I.; Fridovich, I. Stable Mn(Iii) Porphyrins Mimic Superoxide-Dismutase *in-Vitro* and Substitute for It *in-Vivo*. *J. Biol. Chem.* **1994**, *269*, 23471–23476.
51. Szabo, C.; Day, B. J.; Salzman, A. L. Evaluation of the Relative Contribution of Nitric Oxide and Peroxynitrite to the Suppression of Mitochondrial Respiration in Immunostimulated Macrophages Using a Manganese Mesoporphyrin Superoxide Dismutase Mimetic and Peroxynitrite Scavenger. *FEBS Lett.* **1996**, *381*, 82–86.
52. Fridovich, I. Superoxide Radical and Superoxide Dismutases. *Annu. Rev. Biochem.* **1995**, *64*, 97–112.
53. Imlay, J. A.; Fridovich, I. Assay of Metabolic Superoxide Production in *Escherichia coli*. *J. Biol. Chem.* **1991**, *266*, 6957–6965.
54. Zeng, H. Y.; Dvorak, H. F.; Mukhopadhyay, D. Vascular Permeability Factor (VPF)/Vascular Endothelial Growth Factor (VEGF) Receptor-1 Down-Modulates VPF/VEGF Receptor-2-Mediated Endothelial Cell Proliferation, but Not Migration, through Phosphatidylinositol 3-Kinase-Dependent Pathways. *J. Biol. Chem.* **2001**, *276*, 26969–26979.
55. Zeng, H. Y.; Zhao, D. Z.; Yang, S. P.; Datta, K.; Mukhopadhyay, D. Heterotrimeric G Alpha(q)/G Alpha(11) Proteins Function Upstream of Vascular Endothelial Growth Factor (VEGF) Receptor-2 (KDR) Phosphorylation in Vascular Permeability Factor/VEGF Signaling. *J. Biol. Chem.* **2003**, *278*, 20738–20745.
56. Milanini, J.; Vinals, F.; Pouyssegur, J.; Pages, G. p42/p44 MAP Kinase Module Plays a Key Role in the Transcriptional Regulation of the Vascular Endothelial Growth Factor Gene in Fibroblasts. *J. Biol. Chem.* **1998**, *273*, 18165–18172.
57. Mavria, G.; Vercoulen, Y.; Yeo, M.; Paterson, H.; Karasarides, M.; Marais, R.; Bird, D.; Marshall, C. J. ERK-MAPK Signaling Opposes Rho-Kinase to Promote Endothelial Cell Survival and Sprouting During Angiogenesis. *Cancer Cell* **2006**, *9*, 33–44.
58. Oshikawa, J.; Kaplan, N.; Razvi, M.; Urao, N.; McKinney, R.; Fukai, T.; Ushio-Fukai, M. Extracellular SOD-derived H_2O_2 Promotes VEGF Signaling *via* Oxidative Inactivation of Protein Tyrosine Phosphatases Localized in Caveolae/Lipid Rafts. *Circulation* **2009**, *120*, S1020–S1020.
59. Oshikawa, J.; Urao, N.; Kim, H. W.; Kaplan, N.; Razvi, M.; McKinney, R.; Poole, L. B.; Fukai, T.; Ushio-Fukai, M. Extracellular SOD-Derived H_2O_2 Promotes VEGF Signaling in Caveolae/Lipid Rafts and Post-ischemic Angiogenesis in Mice. *PLoS One* **2010**, *5*, e10189–e10189.
60. Arnold, R. S.; Shi, J.; Murad, E.; Whalen, A. M.; Sun, C. Q.; Polavarapu, R.; Parthasarathy, S.; Petros, J. A.; Lambeth, J. D. Hydrogen Peroxide Mediates the Cell Growth and Transformation Caused by the Mitogenic Oxidase Nox1. *Proc. Natl. Acad. Sci. U.S.A.* **2001**, *98*, 5550–5555.
61. Maurer, B. J.; Metelitsa, L. S.; Seeger, R. C.; Cabot, M. C.; Reynolds, C. P. Increase of Ceramide and Induction of Mixed Apoptosis Necrosis by *N*-(4-Hydroxyphenyl)-retinamide in Neuroblastoma Cell Lines. *J. Natl. Cancer Inst.* **1999**, *91*, 1138–1146.

62. Landmesser, U.; Drexler, H. Toward Understanding of Extracellular Superoxide Dismutase Regulation in Atherosclerosis-A Novel Role of Uric Acid? *Arterioscler. Thromb. Vasc. Biol.* **2002**, *22*, 1367–1368.
63. Connor, K. M.; Subbaram, S.; Regan, K. J.; Nelson, K. K.; Mazurkiewicz, J. E.; Bartholomew, P. J.; Aplin, A. E.; Tai, Y. T.; Aguirre-Ghiso, J.; Flores, S. C.; *et al*. Mitochondrial H_2O_2 Regulates the Angiogenic Phenotype *via* PTEN Oxidation. *J. Biol. Chem.* **2005**, *280*, 16916–16924.
64. Bienert, G. P.; Schjoerring, J. K.; Jahn, T. P. Membrane Transport of Hydrogen Peroxide. *Biochim. Biophys. Acta-Biomembr.* **2006**, *1758*, 994–1003.